Ring-polymer molecular dynamics rate-theory in the deep-tunneling regime: Connection with semiclassical instanton theory

Jeremy O. Richardson, and Stuart C. Althorpe

Citation: The Journal of Chemical Physics **131**, 214106 (2009); doi: 10.1063/1.3267318
View online: https://doi.org/10.1063/1.3267318
View Table of Contents: http://aip.scitation.org/toc/jcp/131/21
Published by the American Institute of Physics

Ring-polymer molecular dynamics rate-theory in the deep-tunneling regime: Connection with semiclassical instanton theory

Jeremy O. Richardson and Stuart C. Althorpe
Department of Chemistry, University of Cambridge, Lensfield Road, Cambridge CB2 1EW, United Kingdom

(Received 14 October 2009; accepted 4 November 2009; published online 3 December 2009)

We demonstrate that the ring-polymer molecular dynamics (RPMD) method is equivalent to an automated and approximate implementation of the "Im F" version of semiclassical instanton theory when used to calculate reaction rates in the deep-tunneling regime. This explains why the RPMD method is often reliable in this regime and also shows how it can be systematically improved. The geometry of the beads at the transition state on the ring-polymer potential surface describes a finite-difference approximation to the "instanton" trajectory (a periodic orbit in imaginary time $\beta\hbar$ on the inverted potential surface). The deep-tunneling RPMD rate is an approximation to the rate obtained by applying classical transition-state theory (TST) in ring-polymer phase-space using the optimal dividing surface; this TST rate is in turn an approximation to a free-energy version of the Im F instanton rate. The optimal dividing surface is in general a function of several modes of the ring polymer, which explains why centroid-based quantum-TSTs break down at low temperatures for asymmetric reaction barriers. Numerical tests on one-dimensional models show that the RPMD rate tends to overestimate deep-tunneling rates for asymmetric barriers and underestimate them for symmetric barriers, and we explain that this is likely to be a general trend. The ability of the RPMD method to give a dividing-surface-independent rate in the deep-tunneling regime is shown to be a consequence of setting the bead-masses equal to the physical mass. [doi:10.1063/1.3267318]

I. INTRODUCTION

Ring-polymer molecular dynamics (RPMD) is an approximate method for including quantum effects in time-correlation functions.[1–12] Like the related centroid MD (CMD) method,[13,14] the RPMD method obtains an approximate description of the thermally averaged quantum dynamics by considering the classical dynamics of a set of ring polymers. The ring polymers are the closed loops of replica particles joined by harmonic springs that appear in quantum path-integral simulations of static quantities.[15–22]

The classical dynamics of the ring polymers preserves the quantum Boltzmann distribution and satisfies time-reversal symmetry. These are important properties, but alone they are not sufficient to guarantee that the (fictitious) classical dynamics of the ring polymers gives a realistic approximation to the true quantum dynamics. Nevertheless, both RPMD and CMD have had considerable success. The two methods differ mainly in how they choose the (fictitious) masses of the polymer beads. In RPMD these masses are chosen to be the same as the physical masses of the particles in the system;[1,4] in CMD they are chosen differently[14] such that the fictitious vibrations of the particle springs do not corrupt the vibrational spectrum. As a result, CMD is better than RPMD for simulating spectra.[6,23]

The RPMD method, however, does extremely well when used to calculate thermal reaction rates.[9–12] One can show[9] that the RPMD rate is correct in the classical limit (where each polymer collapses to a point) and that it is also exact for tunneling through a parabolic barrier. The RPMD method can therefore be expected to yield reliable estimates of reaction rates in the classical and shallow-tunneling regimes. However, a surprising result of applying the RPMD method to systems for which accurate quantum rates are available[9,10,12] is that it yields realistic estimates of the rates (usually to within better than a factor of two) at much lower temperatures in the deep-tunneling regime.

In this article, we demonstrate that there is a close link between RPMD rate-theory and the long-established semiclassical instanton approach,[24–32] which explains why the RPMD rate is often reliable in the deep-tunneling regime and also shows how it can be improved. The semiclassical instanton approach belongs to the class of approximate quantum rate methods (for other examples, see Refs. 33–41), which include quantum effects in the Boltzmann operator but treat the dynamics classically. Such methods are expected to yield reliable estimates of the rate, provided it is not influenced by long-time ($t > \beta\hbar$) quantum-coherence effects.

There are two alternative forms of the semiclassical instanton approach, one[24] derived rigorously from the (exact) quantum flux-side correlation function[42] and the other[25–32,43–45] (sometimes called the "Im F" approach) obtained by modeling the rate of transmission through the barrier by the rate of decay of a thermal average of shape resonances (through the same barrier). For a one-dimensional (1D) system, the first approach approximates the rate by

$$k_{\mathrm{inst}}(T)Q_r(T) = (2\pi\hbar^3)^{-1/2}\left|\frac{d^2\widetilde{S}}{d\beta^2}\right|^{1/2}\exp(-\widetilde{S}/\hbar), \tag{1}$$

where $\beta=1/kT$, $Q_r(T)$ is the reactant partition function, and $\widetilde{S}$ is the classical action along the "instanton trajectory." The latter is a periodic orbit in the inverted potential with period $\beta\hbar$. At least one such orbit can be formed at any temperature lower than the "cross-over" temperature $T_c=1/k\beta_c$, where $\beta_c=2\pi/\hbar\omega_b$ and ω_b is the barrier frequency. The second form of instanton theory gives an expression that has the same exponent (containing the action of the instanton) as Eq. (1) but a different prefactor. In practice, the numerical predictions of the two approaches differ usually by a very small amount.[28] The approach of Eq. (1) is clearly to be preferred, as being the more rigorous of the two, but it is the Im F approach that makes clear the link with the RPMD rate and which we will therefore employ here.

The instanton approach often yields reliable predictions of the rates for 1D systems and sometimes for systems with more degrees of freedom, but it suffers from the disadvantage that all degrees of freedom perpendicular to the reaction coordinate are approximated harmonically.[25,39] This is an obvious drawback for significantly anharmonic systems and can also introduce large errors at temperatures just below cross-over.[27] However, there are a variety of generalizations to the instanton approach that do not approximate these degrees of freedom harmonically. These include the "quantum instanton" method of Miller and co-workers,[39] the semiclassical transition-state theory (TST) of Hernandez and Miller,[37] and a free-energy version of the Im F instanton rate derived by Mills *et al.*[29] This last approach turns out to have a very close link to the RPMD rate.

After summarizing previous work on the RPMD approach in Sec. II, we demonstrate in Sec. III that the deep-tunneling RPMD rate is linked closely to the Im F instanton rate and particularly to the free-energy version just mentioned. We investigate the comparison between the RPMD and instanton rates numerically in Sec. IV, where we also explain how to locate approximately the optimal dividing surface in RP space. The derivations in Secs. II–IV are carried out for 1D systems in order to simplify the presentation; extension to multidimensions is straightforward, and we explain how this is done in Sec. V. Section VI concludes the article.

II. RPMD RATE-THEORY

The use of ring polymers to compute statistical averages over time-independent operators is well known and goes back to Feynman.[15–22] The quantum Boltzmann operator in the partition function

$$Q(T) = \mathrm{Tr}[e^{-\beta\hat{H}}] \tag{2}$$

is evaluated in N imaginary time-steps of length $\beta_N=\beta/N$. For a one-dimensional system of mass m, moving in a potential $V(x)$, this gives

$$Q(T) \simeq \left(\frac{m}{2\pi\beta_N\hbar^2}\right)^{N/2}\int d\mathbf{x}e^{-\beta_N U_N(\beta,\mathbf{x})}, \tag{3}$$

where $\mathbf{x}=(x_1,\ldots,x_N)$ and

$$U_N(\beta,\mathbf{x}) = \sum_{n=1}^{N} V(x_n) + \frac{m}{2(\beta_N\hbar)^2}\sum_{n=1}^{N}(x_{n+1}-x_n)^2, \tag{4}$$

where the second sum employs cyclic boundary conditions in n. Equation (3) is very useful since it expresses the quantum statistical average in the form of a classical average in an extended space in which each quantum particle is replaced by a classical ring polymer consisting of N beads. Equation (3) is exact in the limit $N\to\infty$ and generalizes easily to many degrees of freedom.

In RPMD,[1–12] each bead is given an artificial mass equal to the physical mass m and a momentum p_n. This choice of bead-masses is different from that used in the related CMD approach[14] and has been shown[4] to give the best short-time approximation to various Kubo-transformed correlation functions. (In Sec. III F, we will show that this choice of masses also has the important advantage of giving a dividing-surface-independent approximation to the deep-tunneling rate.) The ring polymers are made to follow classical trajectories through the extended phase-space $(\mathbf{x},\mathbf{p})$, subject to the (artificial) Hamiltonian

$$H_N(\mathbf{p},\mathbf{x}) = \sum_{n=1}^{N}\frac{p_n^2}{2m} + U_N(\beta,\mathbf{x}). \tag{5}$$

Similar techniques[17,20–22] have been used as a means of sampling the configuration space $\mathbf{x}$ in calculations of static properties. In RPMD, however, the (artificial) classical dynamics of the beads is taken literally and interpreted as providing an approximation to the exact quantum dynamics of the (real, physical) system. In particular, the RPMD rate $k_{\mathrm{RPMD}}(T)$ is calculated by applying classical rate-theory[46,47] in the space $(\mathbf{x},\mathbf{p})$, which gives[9,10]

$$k_{\mathrm{RPMD}}(T)Q_r(T) = \frac{1}{(2\pi\hbar)^N}\int d\mathbf{p}\int d\mathbf{x}e^{-\beta_N H_N(\mathbf{p},\mathbf{x})} \times\delta[\sigma(\mathbf{x})]v_\sigma(\mathbf{p},\mathbf{x})h[\sigma(\mathbf{x}_t)], \quad t>\tau, \tag{6}$$

with

$$v_\sigma(\mathbf{p},\mathbf{x}) = \left.\frac{d\sigma(\mathbf{x})}{dt}\right|_{t=0} = \frac{1}{m}\sum_{n=1}^{N}\frac{\partial\sigma(\mathbf{x})}{\partial x_n}p_n. \tag{7}$$

The term $\delta[\sigma(\mathbf{x})]v_\sigma(\mathbf{p},\mathbf{x})$ describes the flux of particles through a dividing surface[48] $\sigma(\mathbf{x})=0$ at initial time $t=0$, and the Heaviside step-function $h[\ldots]$ correlates this with the fraction of particles that make it to the product side of the reaction after the "plateau time" τ.[46,47] The RPMD rate is therefore independent of the choice of dividing surface. Most previous implementations[10–12] of Eq. (6) have used a specific form of dividing surface in which σ is taken to be a function of the centroid coordinate $\bar{q}_0$ (see the Appendix). We will use a more general form of dividing surface introduced below.

As mentioned in Sec. I, $k_{\mathrm{RPMD}}(T)$ can be shown to give the correct rate in the classical and parabolic-barrier limits. The main purpose of this article is to explain why it is also a sensible approximation in the deep-tunneling regime at temperatures below T_c, where the parabolic approximation breaks down. To do this, we will need to make use of the TST approximation to Eq. (6),

$$k_{\mathrm{RP\text{-}TST}}(T)Q_r(T) = \frac{1}{(2\pi\hbar)^N}\int d\mathbf{p}\int d\mathbf{x} e^{-\beta_N H_N(\mathbf{p},\mathbf{x})} \times \delta[\sigma(\mathbf{x})]v_\sigma(\mathbf{p},\mathbf{x})h[v_\sigma(\mathbf{p},\mathbf{x})], \quad (8)$$

in which $h[\sigma(\mathbf{x}_t)]$ is approximated by its $t\to 0^+$ limit, $h[v_\sigma(\mathbf{p},\mathbf{x})]$. From classical TST,[46,47] we know that the RP-TST rate $k_{\mathrm{RP\text{-}TST}}(T)$ depends (exponentially) strongly on the location of the dividing surface and that it provides an upper bound to the (non-TST) rate $k_{\mathrm{RPMD}}(T)$. The choice of dividing surface is therefore crucial. In what follows below, we will make extensive use of the *optimal* RP-TST (ORP-TST) rate $k_{\mathrm{ORP\text{-}TST}}(T)$, which we define to be the RP-TST rate obtained using (a sufficiently good approximation to) the optimal choice of dividing surface, i.e., the surface that gives the smallest value of $k_{\mathrm{RP\text{-}TST}}(T)$ and that maximizes the transmission coefficient

$$\kappa(T) = \frac{k_{\mathrm{RPMD}}(T)}{k_{\mathrm{RP\text{-}TST}}(T)}. \quad (9)$$

We will show below that the optimal dividing surface can be approximated by just the centroid coordinate if the reaction barrier is symmetric but that it must be allowed to depend on other normal modes of the ring polymer if it is to yield good approximations to the deep-tunneling rate for asymmetric reaction barriers.

III. CONNECTION WITH SEMICLASSICAL INSTANTON THEORY

A. The Im F approximation

As mentioned in Sec. I, there are two versions of semiclassical instanton theory, and the one that we use here is based on the so-called Im F model.[25–32] The basic assumption behind this model is that one can develop an approximate short-time rate-theory based on the quantum Boltzmann operator in the vicinity of the reaction barrier. Clearly this is true in the classical limit (where the Boltzmann operator is local), and it is reasonable to suppose that it carries over into the quantal deep-tunneling regime where the Boltzmann operator is local to within roughly the thermal wavelength. One is thus free to modify the potential elsewhere, such that it traps the system into a series of resonances, which decay by tunneling through the barrier (as shown schematically in Fig. 1). The tunneling rate is then equal to the thermal average of the rate of decay of the resonances weighted by the (unmodified) reactant partition function and can be written as

$$k(T)Q_r(T) = \frac{1}{\hbar}\sum_k \gamma_k e^{-\beta E_{\mathrm{r}k}}, \quad (10)$$

where $E_{\mathrm{r}k}$ and γ_k are the energies and widths of the resonances.

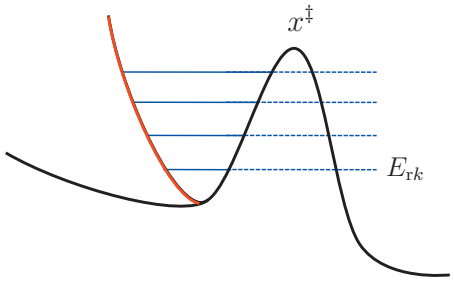

FIG. 1. Schematic illustrating the use of the Im F model to describe a reaction rate in the deep-tunneling regime. The potential energy (black curve) is distorted (red curve) to give a well that accommodates a series of long-lived resonances (blue lines). The decay of the resonances through the barrier gives an approximation to the rate.

Equation (10) is approximate because it neglects the contribution from nonresonant over-the-barrier scattering and also assumes that each resonance has a clearly defined Lorentzian line-shape and width (and there is no guarantee that the surface away from the barrier can be distorted to produce this outcome, although it seems a reasonable possibility). The first of these assumptions will clearly be true at low enough temperatures in the deep-tunneling regime (where the top of the barrier is not thermally accessible). It is also reasonable to suppose that the rate of penetration of the barrier will be very slow in this regime (unless the reaction barrier is atypically thin), in which case one can approximate Eq. (10) by[25–32]

$$k(T)Q_r(T) \approx \frac{2}{\beta\hbar}\mathrm{Im}\, R(T), \quad (11)$$

where

$$R(T) = \sum_k e^{-\beta(E_{\mathrm{r}k} - i\gamma_k/2)}. \quad (12)$$

The set of complex numbers $E_{\mathrm{r}k} - i\gamma_k/2$ can be regarded formally as the discrete spectrum obtained by analytic continuation of the Hamiltonian $\hat{H}$ into the complex plane.[49–51] To derive instanton theory, one applies the analytic continuation directly to the path-integral expression for $Q(T)$, which is straightforward to do if the integrals are approximated using the method of steepest descent.[52] In most of the instanton literature,[26–28] this combination of steepest-descent approximation and analytic continuation is applied to the formally exact expression for $Q(T)$. Here, we apply it to the RP expression of Eq. (3) (which becomes identical to the formally exact expression in the limit $N\to\infty$) in order to demonstrate the connection with the RPMD method.

B. Saddle points on the RP potential surface

The first step in deriving the instanton expression from Eq. (11) is to locate the saddle points on the RP potential surface $U_N(\beta,\mathbf{x})$. From Eq. (4), the stationary points of $U_N(\beta,\mathbf{x})$ satisfy

$$V'(x_n) = m\frac{x_{n+1} - 2x_n + x_{n-1}}{(\beta_N\hbar)^2}, \quad n = 1,\ldots,N. \quad (13)$$

These equations have a trivial solution[28]

$$x_n = x^{\ddagger}, \quad n = 1, \ldots, N, \tag{14}$$

which corresponds to all the normal modes of the ring polymer being zero, except for the centroid mode $\bar{q}_0$ (see the Appendix), which is located at the barrier maximum $x^{\ddagger}$. Above the cross-over temperature T_c, this geometry is the saddle point on $U_N(\beta,\mathbf{x})$, which is consistent with the dynamics of the ring polymer in the classical limit (where it collapses to a point which behaves as a classical particle).

Below T_c, however, the features of $U_N(\beta,\mathbf{x})$ become qualitatively different such that the geometry $x_n = x^{\ddagger}$ is no longer a saddle point. To see why this is so, consider the normal modes at this geometry. Because none of the springs are stretched, the normal modes are identical to those of the free ring polymer (given in the Appendix), except that the normal frequencies are changed to $\sqrt{\omega_k^2 - \omega_b^2}$. Above T_c, $\omega_k > \omega_b$ for all $k \neq 0$, and therefore all the frequencies are real, except for the imaginary frequency $i\omega_b$ associated with the centroid mode. Hence the geometry $x_n = x^{\ddagger}$ is a saddle point. Below T_c, however, $\omega_{\pm 1} < \omega_b$ [see Eq. (A3)], so the modes $q_{\pm 1}$ are now also unstable. Hence the geometry $x_n = x^{\ddagger}$ has three imaginary frequencies and is no longer a saddle point. The unstable modes $q_{\pm 1}$ describe overall stretches of the polymer (see the Appendix), which allow it to lower its energy by "draping" over the top of the barrier.

As a result, the saddle point below T_c corresponds to a nontrivial solution $\mathbf{x} = \tilde{\mathbf{x}}$ to Eq. (13), for which the right-hand side is nonzero. This equation has a very simple physical interpretation since it resembles a finite-difference approximation to Newton's second law, describing the (non-RP) dynamics of the classical particle on the inverted potential $-V(x)$. The nth polymer bead thus gives the position of the particle after n equally spaced time-steps of duration $\beta_N\hbar$. Since the rings are closed and are symmetric under cyclic permutation of the beads, it follows that the classical trajectory that they approximate is periodic, with period $\beta\hbar$. The saddle point $\tilde{\mathbf{x}}$ is therefore a finite-difference approximation to the periodic instanton trajectory.[24] The projections of $\tilde{\mathbf{x}}$ onto the free-polymer normal modes $\mathbf{q}$ are the Fourier components of this trajectory. Examples of the geometry $\tilde{\mathbf{x}}$ obtained for asymmetric and symmetric Eckart barriers are given in Fig. 2.

At temperatures $\beta_c < \beta < 2\beta_c$, the instanton trajectory describes a single "bounce" across the inverted potential in the time $\beta\hbar$. At lower temperatures there is a series of thresholds $\beta = \lambda\beta_c$ (with λ a positive integer), beneath each of which the frequencies of the modes $q_{\pm\lambda}$ become imaginary. This permits the ring polymer to fold back on itself λ times across the top of the barrier, thus representing a periodic trajectory that makes λ bounces in time $\beta\hbar$. In what follows, we will assume that the temperature lies in the single-bounce regime, although the treatment can easily be generalized for lower temperatures. We will refer to the geometry $\tilde{\mathbf{x}}$ of the ring polymer corresponding to the single-bounce trajectory as the "instanton polymer."

The next step in deriving the instanton rate is to compute the normal modes $\{s_k\}$, $k = 0, \ldots, N-1$, and frequencies η_k at the saddle point $\tilde{\mathbf{x}}$, by diagonalizing the Hessian

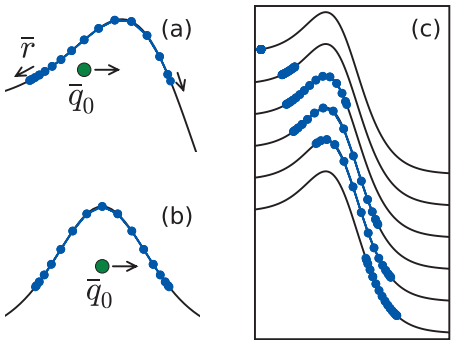

FIG. 2. RP geometries at the instanton saddle point $\tilde{\mathbf{x}}$ for (a) the asymmetric Eckart barrier at $\beta = 10$ a.u. and (b) the symmetric Eckart barrier at $T = 150$ K. The green circles are the positions of the centroids. The arrows represent the dominant contributions to the unstable normal mode, which is a concerted centroid-shift and overall stretch in (a) and just a centroid-shift in (b). Panel (c) shows the RP geometries at various points along the minimum energy path for the asymmetric Eckart barrier at $\beta = 10$ a.u.

$$K_{nn'}(\beta) = V''(\tilde{x}_n)\delta_{nn'} + \frac{m}{(\beta_N\hbar)^2}(2\delta_{nn'} - \delta_{nn'-1} - \delta_{nn'+1}). \tag{15}$$

We define s_0 to be the unstable mode at the saddle point with imaginary frequency $i|\eta_0|$. If s_0 is expanded in a basis of free-polymer normal modes $\mathbf{q}$, then we expect it to be dominated by the imaginary-frequency modes q_0 and $q_{\pm 1}$.

In the derivation of instanton theory based on the exact expression for $Q(T)$,[28] there is a zero-frequency mode s_1, which originates from the invariance of the action $\tilde{S}$ under time translation. In the RP derivation we are following here, the time invariance manifests itself as the symmetry of the potential $U_N(\beta,\mathbf{x})$ under cyclic permutation of the polymer beads. In the limit $N \to \infty$, there is a (circular) degree of freedom, around which $U_N(\beta,\mathbf{x})$ is constant, and which links all cyclic permutations of the N beads. The zero-frequency mode s_1 is tangential to this degree of freedom at the point $\tilde{\mathbf{x}}$. In the $N \to \infty$ limit, therefore, a small displacement in s_1 must move the nth bead at position $\tilde{x}_n$ into position $\tilde{x}_{n+1}$. Hence the $N \to \infty$ limit of s_1 can be written as

$$s_1 = \frac{1}{\sqrt{B_N}} \sum_{n=1}^{N} (\tilde{x}_{n+1} - \tilde{x}_n) x_n, \tag{16}$$

where the normalization coefficient B_N is

$$B_N = \sum_{n=1}^{N} (\tilde{x}_{n+1} - \tilde{x}_n)^2. \tag{17}$$

In a converged numerical calculation, N will be sufficiently large that the frequency $|\eta_1|$ is very small, and the expression in Eq. (16) provides a good approximation to s_1. The higher normal modes $\{s_{k \geq 2}\}$ are all finite and have real frequencies, which tend to the normal modes of the free ring polymer in the limit $k \to \infty$.

C. RP form of the Im F instanton rate

The next step in the derivation[28] is to multiply the RP coordinates by complex scaling factors such that the (real, infinite) partition function $Q(T)$ is transformed into the (complex, finite) quantity $R(T)$ in Eq. (11). The trick[26–28] is to combine this mapping with the evaluation of the integrals over $\mathbf{s}$ by steepest descent. The complex scaling required is then to multiply the unstable mode s_0 by a factor of $i=\sqrt{-1}$ for $s_0>0$ (with s_0 defined such that this direction takes the system away from the potential well shown in Fig. 1). This has the effect of making the frequency η_0 real so that $R(T)$ becomes complex and finite as required. We only require the imaginary part of $R(T)$, which gives the rate through Eq. (11). This part acquires a factor of $\frac{1}{2}$ (since the imaginary part of the Gaussian integral over s_0 is evaluated over half the peak) and is hence given in the steepest-descent approximation by

$$\mathrm{Im}\, R(T) = \frac{N\sqrt{B_N}}{2}\left(\frac{m}{2\pi\beta_N\hbar^2}\right)^{N/2} e^{-\beta_N \tilde{U}_N(\beta)} \times \prod_{k=0}^{N-1}{}' \int ds_k e^{-\beta_N m\eta_k^2 s_k^2/2}, \tag{18}$$

where $\tilde{U}_N(\beta)\equiv U_N(\beta,\tilde{\mathbf{x}})$ and the prime indicates that the zero-frequency mode s_1 has already been integrated out (to give the factor of $N\sqrt{B_N}$) so that $k=1$ is omitted from the product. Evaluation of the Gaussian integrals and substitution into Eq. (11) yield the following expression for the instanton rate:[32]

$$k_{\mathrm{inst}}(T)Q_r(T) = A_N(\beta)e^{-\beta_N \tilde{U}_N(\beta)}, \tag{19}$$

where

$$A_N(\beta) = \frac{1}{\beta_N\hbar}\sqrt{\frac{mB_N}{2\pi\beta_N\hbar^2}}\left|\prod_{k=0}^{N-1}{}'\hbar\eta_k\beta_N\right|^{-1}. \tag{20}$$

This expression tends to the standard Im F form of the instanton rate[28] in the limit $N\to\infty$, where $\beta_N\hbar\tilde{U}_N(\beta)=\tilde{S}$ (the classical action along the instanton trajectory), which gives results which are numerically very close to those of the more rigorous form of instanton theory of Eq. (1).

D. Connection with the harmonic RP-TST rate

To make the link between the instanton and RPMD rates, it is sufficient to note that the derivation just given involves almost the same steps as a derivation of the harmonic approximation to the RP-TST rate. To derive the latter, we identify the same transition state $\tilde{\mathbf{x}}$ with unstable mode s_0 (which is now identified as the "reaction coordinate"), expand the potential to second order in $s_{k\geq 2}$ about $\tilde{\mathbf{x}}$, and compute the free energy at the transition state by integrating out the zero-frequency mode s_1 and evaluating the Gaussian integrals in Eq. (18).

In fact the *only* difference between the harmonic RP-TST derivation and the Im F derivation just given is in the treatment of the unstable mode s_0. As a result, the instanton rate $k_{\mathrm{inst}}(T)$ is related to the harmonic RP-TST rate $k_{h\text{-RP-TST}}(T)$ by

$$k_{\mathrm{inst}}(T) = \alpha_h(T)k_{h\text{-RP-TST}}(T), \tag{21}$$

where

$$\alpha_h(T) = \frac{2\pi}{\beta\hbar|\eta_0|}. \tag{22}$$

At the cross-over temperature T_c, the coefficient $\alpha_h(T)=1$. Hence a harmonic approximation to the RP-TST rate will give a good approximation to the instanton rate at temperatures just below cross-over but will degrade in quality as T_c decreases further. We discuss the behavior of $\alpha_{\mathrm{h}}(T)$ in Sec. IV D.

E. Connection with the RP-TST rate

We now seek an analogous relation to Eq. (21) for the case that the RP-TST rate is evaluated *without* making the harmonic approximation. This would seem to correspond to evaluating $R(T)$ by steepest descent in just the unstable degree of freedom and evaluating the other degrees of freedom exactly. Such a procedure was first carried out (to our knowledge) by Mills *et al.*[29] Equation (3) is written in the form

$$Q(T) = \int_{-\infty}^{\infty} du e^{-\beta F(u)}, \tag{23}$$

where the free energy $F(u)$ is given by

$$F(u) = -\frac{1}{\beta}\ln[Q_{\sigma=u}(T)] \tag{24}$$

and $Q_{\sigma=u}(T)$ is the constrained partition function

$$Q_{\sigma=u}(T) = \frac{1}{(2\pi\hbar)^N}\int d\mathbf{p}\int d\mathbf{x} e^{-\beta_N H_N(\mathbf{p},\mathbf{x})}\delta[\sigma(\mathbf{x})-u]. \tag{25}$$

The coordinate $\sigma(\mathbf{x})$ is chosen to be the unstable degree of freedom for which evaluation of the integral in Eq. (23) by steepest descent about $u=0$ is most accurate. This is equivalent to requiring that $\sigma(\mathbf{x})=0$ defines the optimal dividing surface in a classical TST calculation [since this maximizes $F(0)$]. As a result, there is a close connection between this approach and the ORP-TST rate (i.e., the RP-TST rate evaluated *using the optimal dividing surface*), which is analogous to that between the harmonic RP-TST and instanton rates of Eq. (21). To obtain the free-energy instanton rate, one integrates over u in the same way that one integrated over s_0 in Sec. III C—i.e., one multiplies $u>0$ by i (where this direction is defined to be the one that takes the system out of the well) and makes the steepest-descent approximation. This yields

$$\text{Im } R(T) = \sqrt{\frac{\pi}{2\beta|F''(0)|}} \frac{1}{(2\pi\hbar)^N} \int d\mathbf{p} \int d\mathbf{x} e^{-\beta_N H_N(\mathbf{p},\mathbf{x})} \delta[\sigma(\mathbf{x})]. \tag{26}$$

Substitution of this expression into Eq. (11) yields the free-energy instanton rate $k_{\sigma\text{-inst}}(T)$, which is related to the ORP-TST rate by

$$k_{\sigma\text{-inst}}(T) = \alpha(T) k_{\text{ORP-TST}}(T), \tag{27}$$

where[53]

$$\alpha(T) = \frac{2\pi}{\beta\hbar} \sqrt{\frac{m}{|F''(0)|}}. \tag{28}$$

Hence, in the deep-tunneling regime, the ORP-TST rate $k_{\text{ORP-TST}}(T)$ is a further approximation to the free-energy instanton rate $k_{\sigma\text{-inst}}(T)$ obtained by assuming that $\alpha(T) \simeq 1$. This approximation will hold good at temperatures just below cross-over but will degrade in quality as the temperature is decreased further. Thus it makes sense to compute $k_{\sigma\text{-inst}}(T)$ rather than $k_{\text{ORP-TST}}(T)$ in the deep-tunneling regime unless the computation of the free-energy derivative $F''(0)$ in Eq. (28) is prohibitively expensive. Of course, these relations do not hold *above* the cross-over temperature, where $k_{\text{ORP-TST}}(T)$ is a better approximation to the rate than $k_{\sigma\text{-inst}}(T)$ (since it correctly describes shallow tunneling through the parabolic top of the barrier and tends to the classical TST rate at high temperatures).

F. Connection with the full RPMD rate

The full RPMD rate $k_{\text{RPMD}}(T)$ is related to the RP-TST rate $k_{\text{RP-TST}}(T)$ through Eq. (9). Hence Eq. (27) implies that in the deep-tunneling regime,

$$k_{\text{RPMD}}(T) = \frac{\kappa_Q(T) k_{\sigma\text{-inst}}(T)}{\alpha(T)}, \tag{29}$$

where $\kappa_Q(T)$ is the transmission coefficient for the optimal dividing surface. In the classical and shallow-tunneling regimes, we know that $k_{\text{RPMD}}(T)$ is likely to give a better approximation to the rate than $k_{\text{ORP-TST}}(T)$ since the dynamics of the centroid at these temperatures gives a good description of the physical (classical or parabolic-tunneling) recrossing dynamics. However, the classical dynamics of the polymer beads cannot possibly describe the deep-tunneling recrossing dynamics through the optimal dividing surface. Hence the factor $\kappa_Q(T)$ is fictitious in the deep-tunneling regime, and $k_{\text{RPMD}}(T)$ is therefore an approximation to $k_{\text{ORP-TST}}(T)$.[54]

To clarify this statement, we emphasize that the formal relation between $k_{\text{RPMD}}(T)$ and $k_{\text{ORP-TST}}(T)$ is of course the same in the deep-tunneling regime as at higher temperatures, namely, that $k_{\text{ORP-TST}}(T)$ is an upper bound to $k_{\text{RPMD}}(T)$ and that $k_{\text{RPMD}}(T)$ is independent of the choice of dividing surface. The only thing that is different in the deep-tunneling regime is the *interpretation* of $k_{\text{ORP-TST}}(T)$ and $k_{\text{RPMD}}(T)$. We cannot assign physical meaning to the transmission coefficient $\kappa_Q(T)$ in this regime, but we know that $k_{\text{ORP-TST}}(T)$ is related to $k_{\sigma\text{-inst}}(T)$ through Eq. (27). Hence, we must regard $k_{\text{RPMD}}(T)$ as an approximation to $k_{\text{ORP-TST}}(T)$ in the deep-tunneling regime instead of the other way round. From the formal relation between $k_{\text{ORP-TST}}(T)$ and $k_{\text{RPMD}}(T)$, we know that $k_{\text{RPMD}}(T)$ provides a lower-bound approximation to $k_{\text{ORP-TST}}(T)$. This approximation will be good provided that $\kappa_Q(T) \sim 1$, which will often be the case [unless the classical RP dynamics resembles high-friction Kramers dynamics or some other scenario in which $\kappa_Q(T) \ll 1$].

Although $k_{\text{RPMD}}(T)$ is more approximate than $k_{\text{ORP-TST}}(T)$ in the deep-tunneling regime, it will often be preferable to compute $k_{\text{RPMD}}(T)$ for the obvious reason that this quantity is independent of dividing surface. Of course, a bad choice of dividing surface would correspond to a transmission coefficient $\kappa(T)$ that would be too small to compute efficiently. However, it is often possible to choose a reasonable approximation to the optimal dividing surface and then to compute $k_{\text{RPMD}}(T)$ reasonably efficiently. This strategy has been employed in a number of RPMD calculations to date.[9–12]

The dividing-surface independence of $k_{\text{RPMD}}(T)$ is clearly a major computational advantage, and it is interesting to note that this property follows from the RPMD choice of bead-masses, each of which is set equal to the physical mass. A different choice of bead-masses (such as that used in the CMD method[13,14]) gives an analogous rate to $k_{\text{RPMD}}(T)$, which is also independent of dividing surface. However such a rate does not in general give a lower bound to the ORP-TST rate in the deep-tunneling regime because the position of the optimal dividing surface at these temperatures depends in general on at least several modes of the ring polymer (see Sec. IV) and each of these components will be incorrectly mass-weighted unless the RPMD bead-masses are used. To our knowledge, the RPMD method is the only method able to compute rates in the deep-tunneling regime, which does not require knowledge of the position of an optimal dividing surface.

IV. NUMERICAL COMPARISONS OF RPMD, INSTANTON, AND QUANTUM RATES

In this section, we report numerical tests on one-dimensional model systems in order to investigate the effects of the coefficients $\kappa(T)$ and $\alpha(T)$ on the RPMD rate $k_{\text{RPMD}}(T)$. We also investigate some properties of the instanton polymer transition state at $\tilde{\mathbf{x}}$ and the optimal dividing surface used to calculate the ORP-TST and free-energy instanton rates.

Two sets of calculations were carried out. The first set (Table I) used an asymmetric Eckart barrier

$$V(x) = \frac{A}{1+\exp(-2x/a)} + \frac{B}{\cosh^2(x/a)}, \tag{30}$$

with $A=-18/\pi$, $B=13.5/\pi$, $a=8/\sqrt{3\pi}$ a.u., and a physical mass $m=1$ a.u. These parameters facilitate comparison with the literature[10] and conveniently give a reciprocal cross-over temperature $\beta_c=2\pi$ a.u. The second set of calculations (Table II) used a symmetric Eckart barrier, with $2\pi B/\hbar\omega_b = 12$, $a=0.660\,47$ a.u., and $m=1836$ a.u. These parameters

TABLE I. Tunneling correction factors $c(T)$ for the asymmetric Eckart barrier. The ORP-TST results were obtained using different approximations to the optimal dividing surface $\sigma=0$, in which σ was allowed to depend on (a) just the centroid coordinate $\bar{q}_0$, (b) $\bar{q}_0$ and $\bar{r}$ as in Eq. (33), and (c) all degrees of freedom. The α-ORP-TST results were obtained by multiplying the ORP-TST results in column (b) by the factor $\alpha(T)$ to give the free-energy instanton rate $k_{\sigma\text{-inst}}(T)$ [see Eq. (27)].

		ORP-TST (approx.)					
$\hbar\beta\omega_b$	RPMD	(a)	(b)	(c)	α-ORP-TST$\equiv\sigma$-inst	QM	Inst.
2	1.2	1.2	1.2	1.2	⋯	1.2	⋯
4	2.0	2.0	2.0	2.0	⋯	2.0	⋯
6	5.3	5.6	5.6	5.6	⋯	5.3	⋯
8	28	36	30	29	26	26	28
10	310	540	330	310	250	250	230
12	5900	16 000	6200	6000	4000	4100	3700

facilitate comparison with Ref. 35 and give a cross-over temperature $T_c=239$ K. Both sets of results are presented in the form of tunneling correction factors

$$c(T) = k_{\text{quantum}}(T)/k_{\text{classical}}(T), \tag{31}$$

which are compared with the instanton and exact quantum results.

A. Locating the optimal dividing surface using s_0

To locate a good approximation to the optimal dividing surface (needed to calculate the ORP-TST rate), we used the technique familiar from variational TST (Refs. 55 and 56) in which the free-energy surface is approximated by a plane orthogonal to the unstable mode of the potential energy saddle point; the plane is moved along the unstable mode until the location is found that maximizes the free energy. We need to modify this technique slightly to take into account the zero-frequency mode s_1. As mentioned above, the latter arises because $U_N(\beta,\mathbf{x})$ is invariant under cyclic permutation of the polymer beads. As a result, the optimal dividing surface is conical since it must include the circular degree of freedom that links together all cyclic permutations of the beads. (The conical shape is easy to visualize when using the more approximate form of dividing surface discussed in Sec. IV B.)

Accordingly, we locate an instanton transition state $\tilde{\mathbf{x}}$ corresponding to one particular permutation of the beads using standard saddle point searching techniques.[57,58] We then calculate the free energy by setting the zero-frequency coordinate $s_1=0$, integrating over the resulting $(N-2)$-dimensional plane orthogonal to the unstable mode s_0, and multiplying the integral by $N\sqrt{B_N}$. This last step is equivalent to integrating over the circular degree of freedom linking all cyclic permutations of the beads (see Sec. III B). The free-energy $F(s_0\simeq\sigma)$ is calculated on a grid of points along s_0 in order to find the point $s_0=\Delta s_0$ that (approximately) maximizes the free energy. The resulting tunneling correction factors $c(T)$ are given under column (c) in Tables I and II. [Columns (a) and (b) used more approximate locations of the dividing surface described below.]

The values of Δs_0 and the percentage changes in $k_{\text{ORP-TST}}(T)$ produced by moving the dividing surface from $s_0=0$ to $s_0=\Delta s_0$ are given in Table III for the asymmetric barrier calculation. The biggest changes in $k_{\text{ORP-TST}}(T)$ are produced near the cross-over temperature ($\hbar\beta\omega_b=2\pi$). At these temperatures, the RP potential $U_N(\beta,\mathbf{x})$ flattens out along the path linking $\mathbf{x}^{\ddagger}$ (the saddle point above T_c) to $\tilde{\mathbf{x}}$ (the saddle point below T_c). Away from cross-over, the RP potential becomes tighter, and hence the transition-state geometry becomes closer to the position of the (free-energy) optimal dividing surface.

Comparison of the $k_{\text{RPMD}}(T)$ and $k_{\text{ORP-TST}}(T)$ rates in Tables I and II shows that the effects of recrossing of the optimal dividing surface are small. Further numerical tests will be required to confirm whether this holds true for other systems, especially multidimensional systems in which the potential $V(x)$ is such that a substantial fraction of (non-RP) classical trajectories recross the (non-RP) optimal dividing surface. However, based on Tables I and II, it seems reason-

TABLE II. As Table I, for the symmetric Eckart barrier. The temperature is also given in kelvin to facilitate comparison with previous work (Refs. 10, 35, and 36).

			ORP-TST (approx.)				
T/K	$\hbar\beta\omega_b$	RPMD	(a)	(c)	α-ORP-TST$\equiv\sigma$-inst	QM	Inst.
377	4	1.9	1.9	1.9	⋯	2.1	⋯
301	5	2.7	2.7	2.7	⋯	3.1	⋯
251	6	4.4	4.4	4.4	⋯	5.2	⋯
188	8	17	17	17	21	22	22
150.6	10	100	110	110	140	160	140
125.5	12	1100	1200	1350	1600	2000	1600

TABLE III. Parameters characterizing the optimal dividing surface for the asymmetric Eckart barrier. Δs_0 is the shift along the s_0 axis that maximizes the free energy, and $\%c(T)$ is the resulting percentage change in the tunneling correction factor $c(T)$. ϕ is the pitch of the cone (see Fig. 3).

	β (a.u.)					
	2	4	6	8	10	12
Δs_0 (a.u.)	0.07	0.16	0.34	0.13	0.05	0.01
$\%c(T)$	0.5	5	28	<0.1	<0.1	<0.1
ϕ (°)	0	0	0	32	39	43

able to suppose that the polymer springs do not induce by themselves a significant amount of recrossing of the optimal dividing surface.

B. More approximate expressions for σ

We repeated the ORP-TST calculations using more approximate expressions for the optimal dividing surface. The first of these, which gave the results under column (a) in Tables I and II, is simply

$$\sigma \simeq \bar{q}_0 - \sigma_0, \tag{32}$$

where $\bar{q}_0$ is the centroid (see the Appendix) and the constant σ_0 is chosen such that the (approximate) location of the optimal dividing surface is at $\sigma=0$. With this approximation to the dividing surface, $k_{\text{ORP-TST}}(T)$ reduces to the quantum TST rate of Voth, Chandler, and Miller (VCM),[35,36] and $k_{\sigma\text{-inst}}(T)$ reduces to the rate expression of Gillan.[33,34] Tables I and II are consistent with previous results,[10,35,36] showing that VCM works well above the cross-over temperature T_c but breaks down below T_c for asymmetric barriers. The reason for this behavior is clear from Sec. III: above T_c, the saddle point is the geometry $\mathbf{x}=x^{\ddagger}$, for which the unstable mode is the centroid $\bar{q}_0$. Below T_c, however, the saddle point is the instanton geometry $\tilde{\mathbf{x}}$, for which the unstable mode is s_0. Hence, unless s_0 is dominated by $\bar{q}_0$ (which is not generally the case; see below), Eq. (32) will give a poor approximation to the optimal dividing surface below T_c.

We can, however, generalize Eq. (32) to obtain an expression that continues to work below T_c by expanding σ in terms of the free RP normal modes $\mathbf{q}$ and retaining only the dominant modes. For a one-dimensional system, at reciprocal temperatures between β_c and $2\beta_c$, we expect s_0 and thus σ to be dominated by the imaginary-frequency modes q_0 and $q_{\pm 1}$. We therefore approximate σ by

$$\sigma \simeq \bar{q}_0 \cos\phi + \bar{r}\sin\phi + \sigma_0, \tag{33}$$

where $\bar{r}=\sqrt{(q_1^2+q_{-1}^2)/N}$. The form of $\bar{r}$ takes into account the fact that $U_N(\beta,\mathbf{x})$ is invariant under a cyclic exchange of the beads and thus gives a dividing surface that is conical (in the $N\to\infty$ limit) in the space of q_0 and $q_{\pm 1}$. This is illustrated in Fig. 3. A particular choice of instanton polymer geometry $\tilde{\mathbf{x}}$ corresponds to a point on the cone; the unstable mode s_0 extends radially outward, and the zero-frequency mode s_1 is tangential to the cone (Fig. 3). For an exothermic barrier, $\sin\phi$ is positive such that passage through the dividing surface from reactants to products corresponds to a concerted shift and overall stretch of the instanton polymer [as shown schematically in Fig. 2(a)]. For an endothermic barrier, $\sin\phi$ is negative such that passage through the barrier corresponds to a concerted shift and overall compression.

The results in Table I [under column (b)] show that the simple approximation of Eq. (33) yields values of $k_{\text{ORP-TST}}(T)$, which are very close to those obtained by placing the dividing surface orthogonal to the exact s_0 [column (c) of Table I]. This is true even at temperatures just above the second cross-over temperature ($\beta=4\pi$ a.u.), below which the frequencies of $q_{\pm 2}$ become imaginary (so that these modes also start to contribute significantly to σ). The values taken by ϕ are given in Table III.

For the symmetric barrier, it is easy to show that the symmetry of the Hessian is such that modes q_k with odd and even k cannot mix. The normal modes s_k therefore split into odd and even sets. The reaction coordinate s_0 must be a function of the centroid $\bar{q}_0$ and is therefore a combination of the even modes only. Thus, for a symmetric barrier, Eq. (32) continues to give a good approximation to the optimal dividing surface below T_c (see Table II), which is why the VCM method[35,36] works well for such systems. This approximation would need to be modified below the second cross-over temperature in order to include the modes $q_{\pm 2}$.

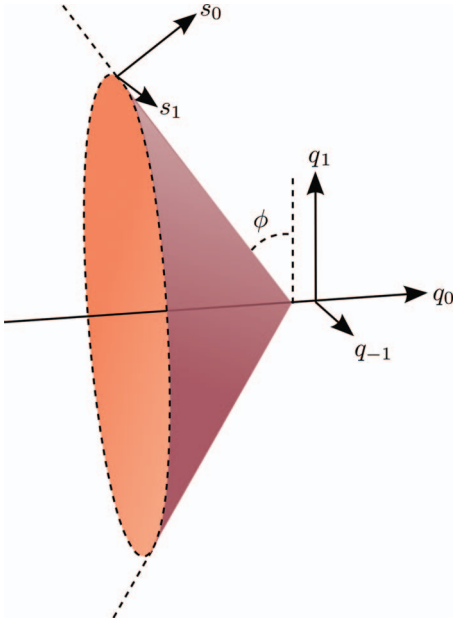

FIG. 3. Approximate form of the optimal free-energy dividing surface for a (one-dimensional) asymmetric barrier. The surface depends on the free-RP normal modes q_0 and $q_{\pm 1}$ and is cone-shaped, owing to the cyclic permutation symmetry of the beads within the polymer. Also shown are the directions of the normal modes s_0 and s_1 at one particular instanton geometry $\tilde{\mathbf{x}}$.

C. Computation of the coefficient $\alpha(T)$

One advantage of using Eq. (33) is that it simplifies the computation of the second derivative of the free energy $F''(0)$, which is required to calculate the parameter $\alpha(T)$ using Eq. (28). From Eq. (24), we can write $F''(0)$ as

$$F''(0) = -\frac{1}{\beta}\frac{Q''_{\sigma=0}(T)}{Q_{\sigma=0}(T)} \tag{34}$$

[since $F'(0)=0$]. On approximating σ by Eq. (33), this expression becomes

$$F''(0) = -\frac{1}{\beta}\left\langle -\beta_N\frac{\partial^2 U_N(\beta)}{\partial\sigma^2} - 2\beta_N\frac{\partial U_N(\beta)}{\partial\sigma}\frac{\sin\phi}{\bar{r}} + \left(\beta_N\frac{\partial U_N(\beta)}{\partial\sigma}\right)^2\right\rangle_{\sigma=0}, \tag{35}$$

where $\langle\ldots\rangle_{\sigma=0}$ denotes a (RP) phase-space average subject to the constraint $\sigma=0$.

Using this approach, it was straightforward to compute $F''(0)$. The constrained averages were computed using the RATTLE algorithm.[59] The α-ORP-TST rates in Table I were obtained by multiplying the resulting $\alpha(T)$ coefficients with the ORP-TST rates from column (b). The α-ORP-TST rates for the symmetric barrier in Table II were obtained by multiplying the ORP-TST rates in column (a) with the $\alpha(T)$ obtained using Eqs. (34) and (35), with $\phi=0$.

D. Predicting the magnitude of $\alpha(T)$

It is clear from Tables I and II that $\alpha(T)$ is likely to be the main source of additional error in the RPMD rate [i.e., on top of any errors already present in the rate $k_{\sigma\text{-inst}}(T)$]. It is therefore useful to predict the likely magnitude of this quantity. From Tables I and II, it is evident that $\alpha(T)$ is roughly equal to unity at the cross-over temperature T_c and that it then decreases with β for the asymmetric barrier (Table I) but increases with β for the symmetric barrier (Table II). These opposite trends are not particular to these two barriers: we have found that they apply generally to symmetric and asymmetric barriers, with weakly asymmetric barriers behaving like symmetric barriers in this respect.

To understand the origin of these trends, we examine the behavior of the coefficient $\alpha_h(T)$ in Eq. (22), which behaves in qualitatively the same way as $\alpha(T)$, provided that $|\eta_0|$ is not too small. This coefficient is exactly unity at the cross-over temperature T_c since at this temperature, $|\eta_0|=2\pi/\beta\hbar$ (by definition). Figure 4 plots the variation in $\alpha_h(T)$ and $|\eta_0|$ with β for the asymmetric and symmetric barriers. For the asymmetric barrier, η_0 changes only slowly with β, with the result that $\alpha_h(T)\sim\beta^{-1}$. For the symmetric barrier, however, η_0 decreases rapidly with β, with the result that $\alpha_h(T)$ increases (roughly linearly) from unity at T_c.

The rapid decrease in $|\eta_0|$ with β for the symmetric barrier occurs because the stretching of the instanton polymer over the top of the barrier flattens out the effective barrier frequency as a function of the centroid coordinate $\bar{q}_0$. Of course the same thing happens for the asymmetric barrier: Fig. 4 shows that the effective barrier frequency as a function of $\bar{q}_0$ drops almost as steeply for the asymmetric as for the symmetric barrier. However, for the asymmetric barrier, s_0 also contains a significant contribution from $q_{\pm1}$ below T_c [by analogy with Eq. (33)], and this contribution increases as the instanton polymer stretches over the barrier and $\omega_{\pm1}^2-\omega_b^2$ becomes more negative. This increasing contribution from the $q_{\pm1}$ modes roughly compensates for the effect of the flattening, with the result that $|\eta_0|$ decreases only slowly with β. For the symmetric barrier, the modes $q_{\pm1}$ are prohibited by symmetry from contributing to s_0, and the contributions from the symmetry-allowed modes $q_{\pm2}$ are too small at these temperatures.

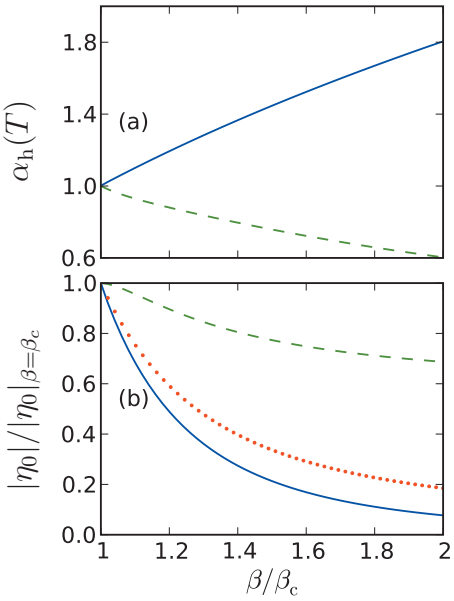

FIG. 4. (a) Variation with β of the coefficient $\alpha_h(T)$ for the asymmetric (dashed green line) and symmetric (blue solid line) Eckart barriers. (b) Variation with β of the unstable frequency $|\eta_0|$ for the asymmetric (dashed green line) and symmetric (blue solid line) barriers. Also shown is the variation with β of the centroid-component of $|\eta_0|$ for the asymmetric barrier (dotted red line).

Hence, for an asymmetric barrier, it is reasonable to assume that

$$\alpha(T) \simeq \frac{\beta_c}{\beta}, \tag{36}$$

which means that $\alpha(T)$ will drop from about 1 to about $\frac{1}{2}$ in the temperature range between β_c and the threshold for secondary instantons (at $2\beta_c$). This is typically the sort of error reported in RPMD rate calculations to date (when accurate quantum results are available for comparison).[9,10,12] For a symmetric barrier, it is more difficult to predict the behavior of $\alpha(T)$, except to say that it will tend to increase with β on account of the flattening-out of the free-energy barrier.

V. MULTIDIMENSIONAL GENERALIZATION

Most of the equations given in the previous sections generalize immediately to multidimensional systems. We illustrate here the changes that need to be made for an f-dimensional system with a classical Hamiltonian of the form

$$H = \sum_{j=1}^{f} \frac{p_j^2}{2m_j} + V(x_1, \ldots, x_f). \tag{37}$$

For such a system, the RP potential $U_N(\beta, \mathbf{x})$ is[10]

$$U_N(\beta, \mathbf{x}) = \sum_{n=1}^{N} V(x_{1,n}, \ldots, x_{f,n}) + \sum_{j=1}^{f} \frac{m_j}{2(\beta_N \hbar)^2} \sum_{n=1}^{N} (x_{j,n+1} - x_{j,n})^2, \tag{38}$$

where $x_{j,n}$ (with $n=1 \rightarrow N$) are the polymer beads associated with classical degree of freedom x_j. The associated RP Hamiltonian is

$$H_N(\mathbf{p}, \mathbf{x}) = \sum_{j=1}^{f} \sum_{n=1}^{N} \frac{p_{j,n}^2}{2m_j} + U_N(\beta, \mathbf{x}), \tag{39}$$

where the $p_{j,n}$ are the momenta of the beads, each of which is assigned a mass m_j (equal to the physical mass). With these changes, the RPMD and RP-TST rate-equations have the same forms as Eqs. (6) and (8), where σ is now in general a function of all $N \times f$ of the coordinates $x_{j,n}$.

The derivation of the Im F instanton rate-expression proceeds exactly as in Sec. III by locating the saddle point on $U_N(\beta, \mathbf{x})$, which is now a finite-difference representation of the f-dimensional instanton trajectory. This trajectory follows a periodic orbit on the inverted potential, with period $\beta\hbar$, which is unstable in the degrees of freedom orthogonal to the reaction coordinate; thus the beads tend to lie on a curve that retraces itself after half a period.[28,32] The f-dimensional instanton polymer has one unstable mode s_0 and a zero-frequency mode s_1. The latter describes a cyclic permutation in which $x_{j,n} \rightarrow x_{j,n+1}$ and thus takes the form

$$s_1 = \frac{1}{\sqrt{B_N}} \sum_{j=1}^{f} \sum_{n=1}^{N} (\tilde{x}_{j,n+1} - \tilde{x}_{j,n}) x_{j,n}, \tag{40}$$

with normalization coefficient

$$B_N = \sum_{j=1}^{f} \sum_{n=1}^{N} (\tilde{x}_{j,n+1} - \tilde{x}_{j,n})^2. \tag{41}$$

The resulting instanton rate $k_{\mathrm{inst}}(T)$ has the same form as Eq. (19), with the prefactor modified to

$$A_N(\beta) = \frac{1}{\beta_N \hbar} \sqrt{\frac{g B_N}{2\pi \beta_N \hbar^2}} \left| \prod_{k=0}^{N-1}{}' \hbar \eta_k \beta_N \right|^{-1}, \tag{42}$$

where

$$g = \left[\prod_{j=1}^{f} m_j \right]^{1/f} \tag{43}$$

and

$$\eta_k = \sqrt{\frac{1}{g} \left| \frac{\partial^2 V}{\partial s_k^2} \right|}. \tag{44}$$

The key relations between $k_{\mathrm{inst}}(T)$ and $k_{h\text{-RP-TST}}(T)$, and between $k_{\sigma\text{-inst}}(T)$ and $k_{\mathrm{ORP\text{-}TST}}(T)$, are exactly as in Eqs. (21) and (27), with the coefficients $\alpha_h(T)$ and $\alpha(T)$ being obtained from the derivatives of the potential with respect to s_0 and the free energy with respect to σ.

Above the cross-over temperature, the optimal dividing surface σ will be a generalized function of the centroids associated with the classical degrees of freedom x_j. In the deep-tunneling regime, σ will in general depend also on the other normal modes of the polymer. This dependency will not necessarily take the simple form of Eq. (33) (for example, the curvature of the potential surface could be sufficiently anharmonic to couple together a variety of RP normal modes), but it is likely to involve only the lowest few normal modes of the polymer. We expect that the trend whereby $\alpha(T)$ decreases with β for an asymmetric barrier and increases with β for a symmetric barrier will continue to hold in multidimensions since if the potential is symmetric (or approximately symmetric) along the reaction coordinate, then the same flattening-out of the free energy will occur, as the polymer extends on either side of the reaction barrier. These properties will need to be investigated numerically in further work.

VI. CONCLUSIONS

We have shown that the RPMD method functions as an automated and approximate implementation of the Im F method when used to calculate reaction rates in the deep-tunneling regime. A major advantage of the RPMD method is that it does not require knowledge of an optimal dividing surface. When the latter is known, however, the ORP-TST rate (the RP-TST rate obtained with the optimal dividing surface) gives a better approximation to the Im F rate than does the RPMD rate. The ORP-TST rate can be further improved by multiplying it by a coefficient that depends on the curvature of the free energy along the reaction coordinate; the resulting rate is then identical to that obtained using a free-energy version of instanton theory.[29] Above the cross-over temperature, the optimal dividing surface is a function of the centroid, but in the deep-tunneling regime the other normal modes of the ring polymer start to participate in the reaction coordinate, beginning with the second-lowest-frequency mode. This explains why VCM quantum TST breaks down for asymmetric barriers in the deep-tunneling regime since the latter method is equivalent to RP-TST, with the optimal dividing surface constrained to be a function of the centroid coordinate only.

These relations and the others explained in the text are summarized in Fig. 5. We should emphasize that this figure applies only in the deep-tunneling regime (the focus of this article). In the shallow-tunneling and classical regimes, the full RPMD rate is of course less approximate than the ORP-TST rate (since it correctly describes recrossing through the optimal dividing surface), and VCM TST can be expected to work also for asymmetric barriers.

The findings of this article add to what is known regarding the relative advantages and disadvantages of the RPMD and CMD methods. It is by now agreed[6,23] that CMD is superior as a method of calculating spectra since it assigns lighter masses to the noncentroid modes of the ring polymer,

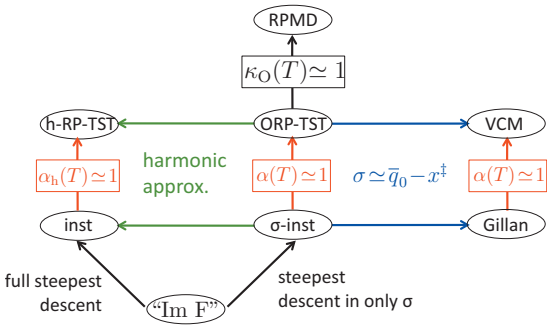

FIG. 5. Diagram summarizing the relations between the various RPMD and instanton rates. All abbreviations and formulae are defined in the text. Each arrow represents an approximation [e.g., the ORP-TST rate is obtained from the σ-inst rate by making the approximation $\alpha(T)=1$]. Note that this diagram applies only to rates calculated in the deep-tunneling regime.

which means that the latter do not corrupt the vibrational spectrum. However, this same choice of masses turns out to be a disadvantage for computing rates. Whereas both RPMD and CMD are likely to yield realistic predictions of the rate above the cross-over temperature (since they are both exact in the classical and parabolic-barrier limits), RPMD is the only method that can be expected to work in the deep-tunneling regime and to yield a prediction of the rate that is independent of the dividing surface used to compute it. The CMD rate is also independent of dividing surface, but is, in general, incorrect in the deep-tunneling regime (since it corresponds to an incorrectly mass-weighted flux through the optimal dividing surface).

The relations established in this article (and summarized in Fig. 5) demonstrate the link between the RPMD method and the Im F premise. However, they do not, as such, demonstrate a link between the RPMD method and the exact quantum rate expression since the Im F premise is, on the basis of present knowledge, merely a model. The model is based on plausible assumptions (see Sec. III), is flexible and general, and, most importantly, appears to work: where exact quantum results are available, the various implementations of the Im F approach (such as the Im F instanton, free-energy instanton, and the RPMD method) give realistic estimates of the rate. However, further investigation into the validity and limitations of the Im F model would clearly be desirable.

ACKNOWLEDGMENTS

It is a pleasure to thank David E. Manolopoulos, William H. Miller, David Chandler, and Thomas Stecher for reading through and commenting on the article. J.O.R. acknowledges a Doctoral Training Account Ph.D. studentship from the UK Engineering and Physical Sciences Research Council.

APPENDIX: NORMAL MODES OF THE FREE RING POLYMER

The normal modes $\mathbf{q}$ of a free ring polymer with N beads have the same form as the eigenstates of an N-membered cyclic Hückel system. For even N they can be written as

$$q_0 = \frac{1}{\sqrt{N}}\sum_{n=1}^{N} x_n,$$

$$q_k = \sqrt{\frac{2}{N}}\sum_{n=1}^{N} \sin\left(\frac{2nk\pi}{N}\right)x_n, \quad k=1,\ldots,(N-2)/2,$$

$$q_{-k} = \sqrt{\frac{2}{N}}\sum_{n=1}^{N} \cos\left(\frac{2nk\pi}{N}\right)x_n, \quad k=1,\ldots,(N-2)/2, \tag{A1}$$

$$q_{N/2} = \frac{1}{\sqrt{N}}\sum_{n=1}^{N} (-1)^n x_n.$$

This last mode is omitted if N is odd. The associated normal frequencies are

$$\omega_{\pm k} = \frac{2N}{\beta\hbar}\sin\left(\frac{|k|\pi}{N}\right). \tag{A2}$$

For low k, the frequencies satisfy

$$\omega_{\pm k} \simeq 2|k|\pi/\beta\hbar \tag{A3}$$

in the limit $N\to\infty$. The centroid $\bar{q}_0$ is the center of mass of the ring polymer, i.e., $\bar{q}_0 = q_0/\sqrt{N}$.

[1] I. R. Craig and D. E. Manolopoulos, J. Chem. Phys. **121**, 3368 (2004).
[2] T. F. Miller III and D. E. Manolopoulos, J. Chem. Phys. **122**, 184503 (2005).
[3] T. F. Miller III and D. E. Manolopoulos, J. Chem. Phys. **123**, 154504 (2005).
[4] B. J. Braams and D. E. Manolopoulos, J. Chem. Phys. **125**, 124105 (2006).
[5] T. E. Markland, S. Habershon, and D. E. Manolopoulos, J. Chem. Phys. **128**, 194506 (2008).
[6] S. Habershon, G. S. Fanourgakis, and D. E. Manolopoulos, J. Chem. Phys. **129**, 074501 (2008).
[7] T. F. Miller III, J. Chem. Phys. **129**, 194502 (2008).
[8] M. Shiga and A. Nakayama, Chem. Phys. Lett. **451**, 175 (2008).
[9] I. R. Craig and D. E. Manolopoulos, J. Chem. Phys. **122**, 084106 (2005).
[10] I. R. Craig and D. E. Manolopoulos, J. Chem. Phys. **123**, 034102 (2005).
[11] R. Collepardo-Guevara, I. R. Craig, and D. E. Manolopoulos, J. Chem. Phys. **128**, 144502 (2008).
[12] R. Collepardo-Guevara, Y. V. Suleimanov, and D. E. Manolopoulos, J. Chem. Phys. **130**, 174713 (2009).
[13] J. Cao and G. A. Voth, J. Chem. Phys. **100**, 5106 (1994).
[14] T. D. Hone, P. J. Rossky, and G. A. Voth, J. Chem. Phys. **124**, 154103 (2006).
[15] R. P. Feynman and A. R. Hibbs, *Quantum Mechanics and Path Integrals* (McGraw-Hill, New York, 1965).
[16] D. Chandler and P. G. Wolynes, J. Chem. Phys. **74**, 4078 (1981).
[17] M. Parrinello and A. Rahman, J. Chem. Phys. **80**, 860 (1984).
[18] D. M. Ceperley, Rev. Mod. Phys. **67**, 279 (1995).
[19] C. Chakravarty, Int. Rev. Phys. Chem. **16**, 421 (1997).
[20] M. E. Tuckerman and A. Hughes, in *Classical and Quantum Dynamics in Condensed Phase Simulations*, edited by B. J. Berne, G. Ciccotti, and D. F. Coker (World Scientific, Singapore, 1998).
[21] D. Marx, M. E. Tuckerman, and G. J. Martyna, Comput. Phys. Commun. **118**, 166 (1999).
[22] C. Chakravarty, J. Chem. Phys. **123**, 024104 (2005).
[23] A. Witt, S. D. Ivanov, M. Shiga, H. Forbert, and D. Marx, J. Chem. Phys. **130**, 194510 (2009).
[24] W. H. Miller, J. Chem. Phys. **62**, 1899 (1975).
[25] S. Chapman, B. C. Garrett, and W. H. Miller, J. Chem. Phys. **63**, 2710 (1975).
[26] C. G. Callan and S. Coleman, Phys. Rev. D **16**, 1762 (1977).
[27] I. Affleck, Phys. Rev. Lett. **46**, 388 (1981).
[28] V. A. Benderskii, D. E. Makarov, and C. A. Wight, Adv. Chem. Phys. **88**,

55 (1994).
[29] G. Mills, G. K. Schenter, D. E. Makarov, and H. Jónsson, Chem. Phys. Lett. **278**, 91 (1997).
[30] Z. Smedarchina, W. Siebrand, and A. Fernández-Ramos, J. Chem. Phys. **127**, 174513 (2007).
[31] G. Mil'nikov and H. Nakamura, Phys. Chem. Chem. Phys. **10**, 1374 (2008).
[32] S. Andersson, G. Nyman, A. Arnaldsson, U. Manthe, and H. Jónsson, Phys. Chem. Chem. Phys. **113**, 4468 (2009).
[33] M. J. Gillan, Phys. Rev. Lett. **58**, 563 (1987).
[34] M. J. Gillan, J. Phys. C **20**, 3621 (1987).
[35] G. A. Voth, D. Chandler, and W. H. Miller, J. Chem. Phys. **91**, 7749 (1989).
[36] G. A. Voth, D. Chandler, and W. H. Miller, J. Phys. Chem. **93**, 7009 (1989).
[37] R. Hernandez and W. H. Miller, Chem. Phys. Lett. **214**, 129 (1993).
[38] T. Yamamoto, H. Wang, and W. H. Miller, J. Chem. Phys. **116**, 7335 (2002).
[39] W. H. Miller, Y. Zhao, M. Ceotto, and S. Yang, J. Chem. Phys. **119**, 1329 (2003).
[40] J. Liu and W. H. Miller, J. Chem. Phys. **131**, 074113 (2009).
[41] J. Shao, J.-L. Liao, and E. Pollack, J. Chem. Phys. **108**, 9711 (1998).
[42] W. H. Miller, S. D. Schwartz, and J. W. Tromp, J. Chem. Phys. **79**, 4889 (1983).
[43] A. O. Caldeira and A. J. Leggett, Ann. Phys. **149**, 374 (1983).
[44] P. Hänggi and W. Hontscha, J. Chem. Phys. **88**, 4094 (1988).
[45] P. Hänggi, P. Talkner, and M. Borkovec, Rev. Mod. Phys. **62**, 251 (1990).
[46] D. Chandler, J. Chem. Phys. **68**, 2959 (1978).
[47] D. Frenkel and B. Smit, *Understanding Molecular Simulation* (Academic, London, 2002).
[48] For simplicity of presentation, we have assumed that the reaction coordinate σ is noncurvilinear; the expression can be generalized to treat a curvilinear reaction coordinate in the usual way (Ref. 47).
[49] E. Balslev and J. M. Combes, Commun. Math. Phys. **22**, 280 (1971).
[50] W. P. Reinhardt, Annu. Rev. Phys. Chem. **33**, 223 (1982).
[51] T. Seideman and W. H. Miller, J. Chem. Phys. **95**, 1768 (1991).
[52] By steepest descent we mean the use of the integral approximation $\int_{-\infty}^{\infty} dx e^{-S(x)/\hbar} \simeq \sqrt{2\pi\hbar/S''(\tilde{x})} e^{-S(\tilde{x})/\hbar}$, where $S(\tilde{x})$ is the minimum of $S(x)$.
[53] The precise form of this expression depends on the mass associated with the reaction coordinate $\sigma(\mathbf{x})$. We have assumed here that $\sigma(\mathbf{x})$ has been normalized such that the associated mass is Nm, which is equivalent to choosing a form of $\sigma(\mathbf{x})$, which becomes independent of N in the limit $N \to \infty$.
[54] The rate $k_{\mathrm{RPMD}}(T)$ may be closer than $k_{\mathrm{ORP\text{-}TST}}(T)$ to the exact quantum rate at some temperatures in the deep-tunneling regime if the factor $\kappa_Q(T)$ happens fortuitously to cancel out errors in $k_{\mathrm{ORP\text{-}TST}}(T)$ [arising from the Im F model and the assumption that $\alpha(T)=1$].
[55] B. C. Garrett, D. G. Truhlar, R. S. Grev, A. W. Magnuson, and J. N. L. Connor, J. Chem. Phys. **73**, 1721 (1980).
[56] D. G. Truhlar, B. C. Garrett, and S. J. Klippenstein, J. Phys. Chem. **100**, 12771 (1996).
[57] J. Nichols, H. Taylor, P. Schmidt, and J. Simons, J. Chem. Phys. **92**, 340 (1990).
[58] C. J. Cerjan and W. H. Miller, J. Chem. Phys. **75**, 2800 (1981).
[59] H. C. Andersen, J. Comput. Phys. **52**, 24 (1983).